



# Adsorption of organic contaminants on biochar colloids: effects of pyrolysis temperature and particle size

Rashida Hameed<sup>1</sup> · Cheng Lei<sup>1</sup> · Daohui Lin<sup>1,2</sup>

Received: 29 December 2019 / Accepted: 2 March 2020 / Published online: 18 March 2020  
© Springer-Verlag GmbH Germany, part of Springer Nature 2020

## Abstract

Biochar (BC) colloids attract increasing interest due to their unique environmental behavior and potential risks. However, the interaction between BC colloids and organic contaminants that may affect their fates in the environment has not been substantially studied. Herein, adsorption and desorption of phenanthrene (PHN), atrazine (ATZ), and oxytetracycline (OTC) by a series of BC colloids derived from bulk rice straw BC samples with 6 pyrolysis temperatures (200–700 °C), and 3 particle sizes (250 nm, 500 nm, and 1 μm) were investigated. Regardless of pyrolysis temperature, BC colloids from a given sized bulk BC had a comparable size, being  $30 \pm 6$ ,  $70 \pm 18$ , and  $140 \pm 15$  nm corresponding to the three sized bulk BCs, respectively. The adsorption kinetics curves were well explained by the pseudo-second-order model, and pore diffusion was the primary rate-determining step. Both Freundlich and Langmuir models well fitted the adsorption isotherms. With increasing pyrolysis temperature or decreasing particle size of bulk BC, the specific surface area and pore volumes of the derived BC colloids increased, the kinetics model fitted adsorption rates ( $k_2$ ) of the three organics by the BC colloids all largely decreased, and the Langmuir model fitted adsorption capacities ( $Q_{\max}$ ) increased. The highest  $Q_{\max}$  was obtained by BC colloids from the smallest (250 nm) bulk BC with the highest pyrolysis temperature (700 °C), being  $212 \mu\text{mol g}^{-1}$  for PHN,  $815 \mu\text{mol g}^{-1}$  for ATZ, and  $72.4 \mu\text{mol g}^{-1}$  for OTC. The adsorption was reversible for PHN and ATZ, while significant desorption hysteresis was observed for OTC on BC colloids with middle pyrolysis temperatures (300–500 °C). The underlying mechanisms including hydrophobic interaction,  $\pi$ - $\pi$  electron donor-acceptor interaction, molecular size effect, and irreversible reactions were discussed to explain the difference in the adsorption and desorption behaviors. The findings increased our understanding of the environmental fate and risk of BC.

**Keywords** Colloidal biochar · Organic contaminants · Adsorption · Desorption hysteresis

## Introduction

Biochar (BC) has gained significant attention due to its great application potential for environmental remediation, carbon

sequestration, agriculture improvement, and energy production (Lehmann and Joseph 2009; Ahmad et al. 2014). Bulk BC particles can be physically degraded into microscale or nanoscale colloids in the environment (Spokas et al. 2014). Distinguished from bulk BC, BC colloids present excellent mobility in the environment (Zhang et al. 2010; Major et al. 2010). Besides, owing to the large specific surface area and extensive functional groups inherited from bulk BC, BC colloids are anticipated to have superior adsorption capacity to various inorganic and organic contaminants (Major et al. 2010). Thus, BC colloids can likely act as a carrier for organic and inorganic contaminants (Wang et al. 2013) and may bring threats to the environment. It is thus urgent to understand the interaction between BC colloids and contaminants.

There is no doubt that the properties of BC colloids can play a vital role in the interaction between BC colloids and contaminants. BC colloids mainly come from pyrolysis-

---

Responsible editor: Zhihong Xu

**Electronic supplementary material** The online version of this article (<https://doi.org/10.1007/s11356-020-08291-5>) contains supplementary material, which is available to authorized users.

✉ Daohui Lin  
lindaohui@zju.edu.cn

<sup>1</sup> Department of Environmental Science, Zhejiang University, Hangzhou 310058, China

<sup>2</sup> Zhejiang Provincial Key Laboratory of Organic Pollution Process and Control, Zhejiang University, Hangzhou 310058, China

induced pore collapse, matrix fracture during BC preparation, and the physical breakup of BC by grinding (Liu et al. 2018). Hence, the properties of BC colloids are inherited from the bulk BC. It was observed that BC colloids released from a hardwood bulk BC (pyrolyzed at 500 °C) by water erosion showed no detectable alteration in O/C atomic ratio relative to the bulk BC (Spokas et al. 2014). Conversely, different results have also been reported. For example, BC fractions below 0.45  $\mu\text{m}$  contained more polar groups and less aromatic clusters than the larger BCs (1–150  $\mu\text{m}$ ) produced from rice straw and bamboo at 400 °C (Qu et al. 2016); BC colloids from a peanut shell BC contained more oxygen and fewer aromatic structures than the bulk BC (Liu et al. 2018); BC colloids from the bulk BC with lower pyrolysis temperature had more carboxyl and hydroxyl groups and thereby exhibited higher removal of heavy metal ions (Qian et al. 2016). These studies filled in the gap of fundamental knowledge about the property and behavior of BC colloids. However, more studies are still needed to address the interaction between BC colloids and organic contaminants, especially the effects of pyrolysis temperature and particle size of bulk BC.

In addition to the inherent properties of BC colloids, their interactions with organic contaminants and the involved mechanisms can vary with the molecular structure and property of organics. Various mechanisms including hydrophobic, electrostatic,  $\pi$ – $\pi$  electron donor and accept, and hydrogen bonding interactions have been reported to regulate the adsorption of organic contaminants, such as phenanthrene (PHN) (Xie et al. 2014; Zhu and Pignatello 2005), oxytetracycline (OTC) (Ji et al. 2009; Oleszczuk et al. 2009), and atrazine (ATZ) (Zhao et al. 2013a, b) by bulk BCs. However, BC colloids with more or less different properties (e.g., size, pore structure, and/or surface chemistry) from their bulk ones can likely have different adsorption behaviors, and this difference may be organics-dependent. Moreover, knowledge on the desorption of organics from BC colloids is still waiting to be filled in. It has been implied that the occurrence of desorption hysteresis would greatly affect the fate and toxicity of organics associated with BC colloids (Mukherjee et al. 2016). Thus, it is crucial to elucidate the relationship between the properties of organics and the adsorption-desorption behaviors of BC colloids.

Herein, we systematically investigated the adsorption-desorption behaviors of PHN, OTC, and ATZ on BC colloids from rice straw bulk BCs with different pyrolysis temperatures and particle sizes. The main objectives were (a) to illustrate the effect of pyrolysis temperature and particle size of bulk BCs on the adsorption behavior of the derived BC colloids; (b) to address the effect of organics properties on the adsorption; and (c) to explore the desorption hysteresis and its relationship with the properties of BC colloids and organics.

## Material and methods

### Preparation and characterization of BC colloids

Bulk BC samples had been prepared and used in our previous study (Hameed et al. 2019). Briefly, cleaned and dried rice straw biomass was charred in a muffle furnace (SX2-12-10, Ningbo Hinotek Technology Co., China) under the oxygen-limited condition at 200, 300, 400, 500, 600, and 700 °C for 6 h to obtain BC samples with various pyrolysis temperatures. The BC samples were then ground, sieved through 2 mm mesh, and labeled as BC200, BC300, BC400, BC500, BC600, and BC700, respectively. A portion of the sieved BC samples were further milled by a high energy planetary ball mill (QM-3SP2, T-Bota Scitech, Nanjing, China) at 40 Hz for 1, 6, and 18 h to obtain the target sizes of 1  $\mu\text{m}$  (BC<sub>1  $\mu\text{m}$</sub> ), 500 nm (BC<sub>500 nm</sub>), and 250 nm (BC<sub>250 nm</sub>), respectively.

BC colloids were obtained from the above bulk BC samples with different pyrolysis temperatures and particle sizes following the study of Qian et al. (2016). Briefly, 2 g of bulk BC were added in 200 mL of ultrapure water, sonicated (100 W, 45 kHz, KQ-800VDB sonicator, Kunshan, China) for 30 min, and followed by settling for 24 h to extract BC colloids. Afterwards, BC colloids in the supernatant were collected by centrifugation (1000g, 30 min) and drying in an oven (105 °C, 24 h) for subsequent characterization and adsorption experiments.

The size and morphology of BC colloids were analyzed by transmission electron microscopy (TEM, JEM-2010, JEOL, Japan). The elemental contents of C, H, and N were measured by an elemental analyzer (MicroCube, Elementar, Germany), and the O content was determined by mass balance (Chen et al. 2008). The atomic ratios of H/C and (O + N)/C were calculated to evaluate the aromaticity and polarity of BC colloids, respectively (Lin et al. 2007). Ash content was obtained by the combustion of BC colloids at 750 °C for 6 h (ASTM 1989). A physisorption analyzer (Quantchrome AUTOSORB AS-1) was applied to measure specific surface areas and pore volumes of BC colloids. Specific surface area (SA) was calculated by BET method, micropore surface area ( $A_{\text{micro}}$ ) was calculated by V-t method, micropore volume ( $V_{\text{micro}}$ ) and total pore volume (PV) were calculated by DFT method, and mesopore volume ( $V_{\text{meso}}$ ) was calculated by subtracting  $V_{\text{micro}}$  from PV. To understand the carbon structure of BC colloids, Raman spectra were obtained by using a confocal Raman microscope (LabRAM HR Evolution, HORBA Jobin Yvon Inc., France) with an Ar<sup>+</sup> laser (514 nm, 10 mW) at a nominal resolution of 3–5  $\text{cm}^{-1}$  within 4000–400  $\text{cm}^{-1}$ . Solid-state cross-polarization magic angle spinning and total sideband suppression <sup>13</sup>C nuclear magnetic resonance (NMR) spectra of BC colloids were acquired with a NMR spectrometer (Bruker Avance 300 MHz, Karlsruhe, Germany) equipped with a 4-mm H-X MAS probe. NMR

spectra were integrated to identify the structural modification of carbon into the following chemical shift regions: aliphatic C (0–109 ppm), aromatic C (109–163 ppm), and polar C (50–109 and 145–220 ppm) (Lin et al. 2007). Surface functional groups of BC colloids were analyzed by using Fourier transform infrared spectroscopy (FTIR, Thermo Scientific Nicolet IS5) with a resolution of  $2\text{ cm}^{-1}$  from  $4000$  to  $400\text{ cm}^{-1}$ .

## Adsorbates

Analytical grade phenanthrene (PHN), atrazine (ATZ), and oxytetracycline (OTC) were all obtained from Aladdin Chemicals Reagent Company (Shanghai, China). The three chemicals have distinct physicochemical properties as listed in Table S1 in the Supporting Information (SI), and they are typical representatives of polyaromatic hydrocarbons, pesticides, and antibiotics, respectively.

## Adsorption experiments

A series of batch adsorption experiments were conducted at  $25 \pm 1\text{ }^\circ\text{C}$ .  $\text{CaCl}_2$  solution ( $0.01\text{ M}$  in ultrapure water, pH 7) was used as the background solution to maintain a constant ionic strength during the adsorption. The solution pH kept largely stable during the adsorption, with the equilibrium pH within 7–8. PHN and ATZ were first dissolved in methanol and then diluted by the background solution to desired concentrations. Methanol concentration in the final solutions was kept  $< 0.1\%$  to avoid the potential co-solvent effect. Adsorptive OTC solutions were directly prepared by dissolving different amounts of OTC in the background solution. Due to the difference in solubility and adsorption capacity, 8, 40, and  $100\text{ mL}$  of adsorptive solutions were used for OTC, ATZ, and PHN, respectively. The mixtures were agitated on a rotary shaker ( $150\text{ rpm}$ ,  $25\text{ }^\circ\text{C}$ ) in the dark. For adsorption kinetics, the initial concentrations of OTC, ATZ, and PHN were  $10$ ,  $10$ , and  $0.5\text{ mg L}^{-1}$ , respectively, and the shaking was maintained for 0–120 h. For adsorption isotherms, the experiments were performed with  $1\text{--}30\text{ mg L}^{-1}$  OTC,  $1\text{--}30\text{ mg L}^{-1}$  ATZ, and  $0.05\text{--}1\text{ mg L}^{-1}$  PHN. The used dosages of BC colloids varied with their adsorption capacities for different organics, achieving an equilibrium removal rate of ca. 20–80% within 5 days. The dosages were 5, 4, and  $2\text{ mg}$  for BC colloids from BC200–300, BC400–500, and BC600–700, respectively. After the adsorption, the mixtures were centrifuged ( $3500\text{g}$ ,  $10\text{ min}$ ), and the supernatants were collected to determine the remaining concentration of target organics. The adsorption kinetics and isotherm experiments were all run in duplicate, including blank controls without BC colloids. The adsorption amount was calculated by the mass difference before and after the adsorption due to the negligible organics loss ( $< 4\%$ ) during the adsorption.

## Adsorption data fitting

The Lagergren pseudo-first-order (Eq. 1) and pseudo-second-order (Eq. 2) models were used to fit the adsorption kinetics data.

$$\ln(q_e - q_t) = \ln q_e - k_1 t \quad (1)$$

$$\frac{t}{q_t} = \frac{1}{k_2 q_e^2} + \frac{t}{q_e} \quad (2)$$

where  $q_e$  and  $q_t$  ( $\mu\text{mol g}^{-1}$ ) are the amounts of adsorbed chemicals at equilibrium and at a given time point  $t$ , respectively, and  $k_1$  ( $\text{min}^{-1}$ ) and  $k_2$  ( $\text{g } \mu\text{mol}^{-1} \text{min}^{-1}$ ) are the adsorption rate constants of the pseudo-first-order and pseudo-second-order models, respectively.

Adsorption isotherms were fitted by the Freundlich (Eq. 3) and Langmuir (Eq. 4) models.

$$q_e = K_F C_e^n \quad (3)$$

$$Q_e = Q_{\max} K_L C_e / (1 + K_L C_e) \quad (4)$$

where  $C_e$  ( $\mu\text{mol L}^{-1}$ ) is the aqueous concentration of chemicals at equilibrium,  $K_F$  ( $\mu\text{mol}^{1-n} \text{g L}^{-n}$ ) is the Freundlich isotherm affinity coefficient,  $n$  (dimensionless) is the isotherm nonlinearity index,  $K_L$  ( $\text{L } \mu\text{mol}^{-1}$ ) is the Langmuir sorption coefficient, and  $Q_{\max}$  ( $\mu\text{mol g}^{-1}$ ) is the sorption capacity.

## Desorption experiment

Desorption experiments were conducted immediately after the adsorption isotherm experiments. The supernatants of the adsorptive solutions were decanted after centrifugation ( $3500\text{g}$ ,  $10\text{ min}$ ) and replaced with the equivalent amount of the background solution. The vials were resealed and shaken for another 5 days to reach equilibrium. The mixtures were then centrifuged, and the supernatants were collected to analyze the concentrations of chemicals in the aqueous phase.

To quantitatively evaluate the desorption hysteresis, hysteresis index (HI) was calculated as follows (Huang et al. 1998).

$$\text{HI} = \frac{q_e^d - q_e^s}{q_e^s} | C_e \quad (5)$$

where  $q_e^d$  and  $q_e^s$  are the equilibrium chemical concentrations in solid phase for the desorption and adsorption experiments, respectively, and the subscript  $C_e$  specifies constant conditions of residual solution phase concentration. The HI indices were calculated for BC colloids from BC<sub>1</sub>  $\mu\text{m}$ , and  $C_e = 0.5, 10,$  and  $3\text{ } \mu\text{mol L}^{-1}$  for PHN, ATZ, and OTC, respectively, were selected for the calculation because these concentration points were within the sharp increasing slope of isotherms of the respective organics and the potential desorption hysteresis if existed would be significant.

## Analytical methods

The collected supernatant samples from the adsorption and desorption experiments were filtered (0.22  $\mu\text{m}$ ) and analyzed by a reverse-phase high-performance liquid chromatography (HPLC, Shimadzu, LC-20A series, Japan) equipped with a XDB-C18 column (4.6  $\times$  150 mm) (Zhao et al. 2013a, b; Wang et al. 2017; Yang et al. 2016). PHN was determined by a fluorescence detector (Shimadzu, RF-5301PC, Japan) with excitation and emission wavelengths of 366 nm and 350 nm, respectively, and the mobile phase was composed of 90% methanol and 10% water. ATZ was measured by a UV detector at 222 nm (Shimadzu, UV-2450, Japan), and a mixture of 80% methanol and 20% water was used as the mobile phase. The absorbance at 360 nm and a mobile phase of 80% methanol and 20% water with 0.02 M phosphoric acid were applied to determine OTC with the HPLC. The flow rates of mobile phases were all set at 1.0 mL min<sup>-1</sup>, and the column temperature was kept at 40 °C.

## Statistical analysis

Correlation analysis was performed to establish the relationship between physicochemical properties of BCs colloids and  $Q_{\text{max}}$ . A one-way analysis of variance (ANOVA) was carried out to study the significant difference between two sets of data, with  $p < 0.05$  defined as significant.

## Results and discussion

### Characteristics of BC colloids

The collected BC colloids from different sized bulk BCs with various pyrolysis temperatures are shown in Fig. 1 and Fig. S1 in SI. The BC colloids were all roughly spherical. Independent of pyrolysis temperature, BC colloids derived from a given sized bulk BC had a comparable size, and the measured colloidal size increased with the size of bulk BC, being  $30 \pm 6$ ,  $70 \pm 18$ , and  $140 \pm 15$  nm ( $n > 100$ ) for the colloids from bulk BC<sub>250 nm</sub>, BC<sub>500 nm</sub>, and BC<sub>1  $\mu\text{m}$</sub> , respectively. The elemental compositions of BC colloids from bulk BCs with a same pyrolysis temperature were comparable and independent on particle size (Table S2), which was also largely the same as that of bulk BCs as determined in our previous study (Hameed et al. 2019). With increasing pyrolysis temperature for bulk BC, the C content of derived BC colloids increased ( $p < 0.05$ ), while atomic ratios of O/C, H/C, and (O + N)/C of BC colloids decreased gradually. This indicates that BC colloids received a higher degree of carbonization and aromaticity but lower polarity from bulk BC with higher pyrolysis temperature (Lin et al. 2007; Chen et al. 2008).

BC colloids from bulk BCs with a same pyrolysis temperature showed similar FTIR (Figs. 2a and S2) and Raman (Figs. 2b and S3) spectra regardless of their different particle sizes. The variation in FTIR spectra of BC colloids as a function of pyrolysis temperature is shown in Fig. 2a. The bands at 1058–1160 cm<sup>-1</sup> were attributed to C–O–C bond, indicating the presence of oxygen containing functional groups in BC colloids (Chen et al. 2008). The peaks for O–H (3404 cm<sup>-1</sup>), C–H (2931 and 2854 cm<sup>-1</sup>), and C=O (1719 cm<sup>-1</sup>) lost their intensities with increasing pyrolysis temperature of bulk BC and nearly disappeared in BC700-derived colloids. In contrast, the bands for C=C stretching (1605 cm<sup>-1</sup>) and Si–O–Si stretching (490 cm<sup>-1</sup>) became more obvious with the elevated pyrolysis temperature for bulk BC. Raman spectra of BC colloids (Figs. 2b and S3) showed remarkable D (1350 cm<sup>-1</sup>) and G (1580 cm<sup>-1</sup>) bands, corresponding to amorphous sp<sup>3</sup> and graphitic sp<sup>2</sup> carbon structures, respectively (Ferrari 2007). The intensity ratio of D to G bands ( $I_D/I_G$ ) increased with increasing pyrolysis temperature, indicating the carbon defect of BC colloids increased as the pyrolysis temperature increased (Zhang et al. 2012). The solid-state <sup>13</sup>C NMR spectra (Fig. 2c) depicted that the BC colloids from the bulk BC pyrolyzed at 200 °C had relatively high aliphatic carbon fractions, including paraffinic or alkyl (27 ppm), methoxyl (68 ppm), O-alkylated (HCOH) (73 ppm), and anomeric O–C–O (103 ppm) carbons, while these aliphatic peaks disappeared and the peaks for aromatic carbon (118–130 ppm) dominated in the NMR spectra of BC colloids derived from bulk BCs with higher pyrolysis temperature (Lin et al. 2007). The above results demonstrated that oxygen-containing functional groups decreased, while aromaticity increased for BC colloids from bulk BCs with increasing pyrolysis temperature, which is quite similar to the effect of pyrolysis temperature on bulk BCs in our previous study (Hameed et al. 2019).

The specific surface area and pore volumes of BC colloids increased with increasing pyrolysis temperature or decreasing particle size of bulk BC (Table 1). Both micropores and mesopores contributed to the total pore volume of BC colloids from bulk BCs with high pyrolysis temperatures, while mesopores became the primary contributor in BC colloids with low pyrolysis temperature. This was understandable because the melting and softening of biomass components at low pyrolysis temperature may partly block the pores and thereby decrease the surface area (Liu et al. 2010). Higher pyrolysis temperature could facilitate the removal of aliphatic and volatile components, rendering BC colloids with greater surface area and pore volume (Agrafioti et al. 2013).

### Adsorption kinetics

The adsorption kinetics of PHN, ATZ, and OTC on BC colloids are shown in Figs. 3 and S4, S5, and S6. The pseudo-



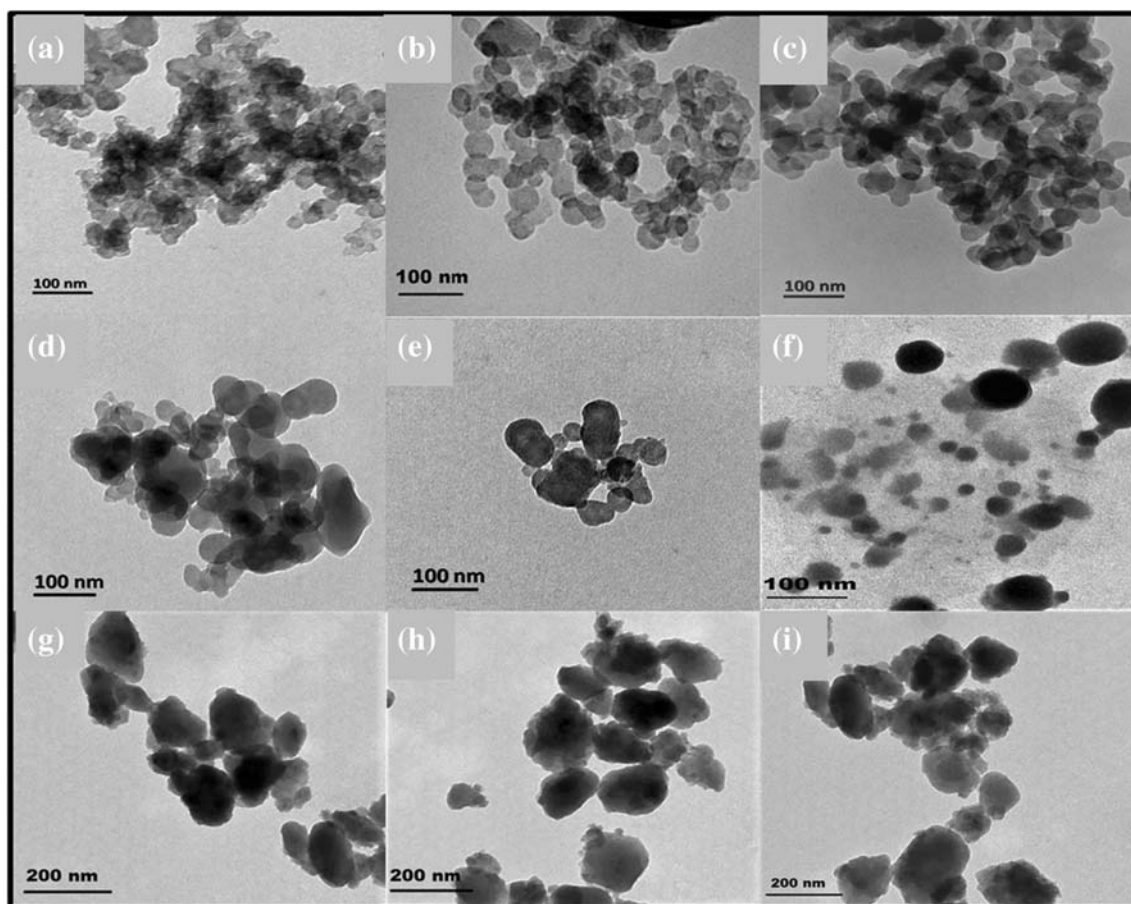


**Fig. 1** Representative TEM images of BC colloids released from BC<sub>250 nm</sub> (a, b, and c), BC<sub>500 nm</sub> (d, e, and f), and BC<sub>1 μm</sub> (g, h, and i) with the pyrolysis temperatures of 200 °C (a, d, and g), 400 °C (b, e, and h), and

600 °C (c, f, and i). More TEM images for other BC colloids are shown in Fig. S1 in SI

second-order model provided better fitness to the kinetics curves compared with the pseudo-first-order model as indicated by the relatively higher  $R^2$  of the former (Table S3). The adsorption rates ( $k_2$ ) of the organics by BC colloids all largely decreased with pyrolysis temperature increasing from 200 to 700 °C. The pyrolysis temperature-dependent difference in porosity and structure of BC colloids could cause the difference in the adsorption kinetics. The organic carbon in BC colloids with higher pyrolysis temperature was more condensed, which could form highly cross-linked micropores and impede the pore diffusion of sorbate molecules, resulting in the lower adsorption rates (Fu et al. 2018). However, for BC colloids with low pyrolysis temperature, the adsorption of organics could be dominated by dissolution (partitioning) in non-condensed organic and amorphous carbon, which was relatively fast (Jones and Tiller 1999; Schlautman and Morgan 1993).

At a fixed pyrolysis temperature, BC colloids from smaller bulk BC presented lower  $k_2$  for the organics (Table S4). For example,  $k_2$  decreased from 0.008 to 0.005, 0.0006 to 0.0001, and 0.005 to 0.002 g μmol<sup>-1</sup> min<sup>-1</sup> for PHN, ATZ, and OTC, respectively, as the size of bulk BC decreased from 1 μm to

250 nm. This could be because smaller BC colloids had larger specific surface area and pore volume and thereby needed a longer time to reach the adsorption equilibrium.

### Adsorption isotherms

Adsorption isotherms of PHN, ATZ, and OTC on BC colloids are shown in Figs. 4 and S7, S8, and S9. The Freundlich and Langmuir models fitted parameters are summarized in Table S4. Both models very well fitted the isotherms with  $R^2$  ranging from 0.88 to 0.99. The very low  $n$  values (0.25–0.46) as fitted by the Freundlich model indicated the nonlinear adsorption of the organics on BC colloids and the existence of condensed or glassy organic domains in the colloids (Wang and Xing 2007). The Langmuir model fitted  $Q_{\max}$  for the organics increased significantly with increasing pyrolysis temperature of BC colloids at a given particle size. For example,  $Q_{\max}$  of BC colloids from BC200–BC700 (1 μm) was 26.1–138 μmol g<sup>-1</sup> for PHN, 227–673 μmol g<sup>-1</sup> for ATZ, and 8.80–31.1 μmol g<sup>-1</sup> for OTC, respectively.  $Q_{\max}$  also significantly increased with decreasing particle size of BC colloids at a given pyrolysis temperature. For example, the highest  $Q_{\max}$

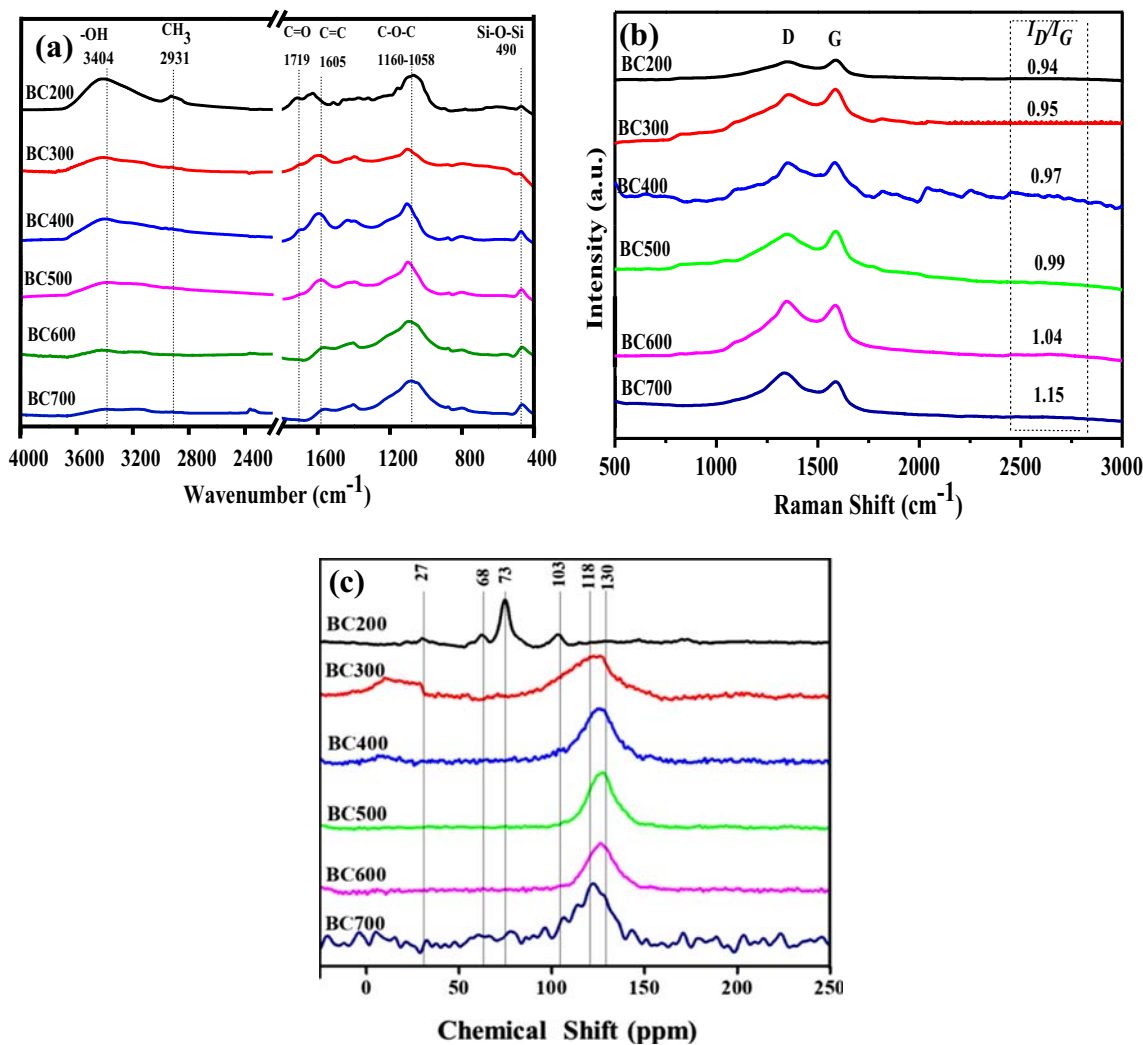


**Fig. 2** **a** FTIR spectra, **b** Raman spectra, **c** solid-state <sup>13</sup>C NMR spectra of BC colloids from BC<sub>1 μm</sub> with different pyrolysis temperatures. FTIR and Raman spectra of BC colloids from BC<sub>250 nm</sub> and BC<sub>500 nm</sub> are given in Figs. S2 and S3 in SI, respectively

was observed for BC colloids from BC700 of 250 nm (ATZ, 815 μmol g<sup>-1</sup>; PHN, 212 μmol g<sup>-1</sup>; OTC, 72.6 μmol g<sup>-1</sup>), which was much higher than that for BC colloids from BC700 of 1 μm (ATZ, 672 μmol g<sup>-1</sup>; PHN, 138 μmol g<sup>-1</sup>; OTC, 31.1 μmol g<sup>-1</sup>). The variation trend in *Q*<sub>max</sub> of BC colloids with pyrolysis temperature or particle size is consistent with that of bulk BCs as well reported elsewhere (Chen et al. 2008; Wang et al. 2017; Yah et al. 2016) and can be explained by the larger specific surface area and pore volume of BCs with higher pyrolysis temperature or smaller particle size. Notably, all BC colloids exhibited much higher *Q*<sub>max</sub> for ATZ than that for PHN and OTC, which is discussed in detail in “Adsorption-desorption mechanisms for the three organics”.

To reveal the relationship between *Q*<sub>max</sub> and BC colloid properties, the correlations between *Q*<sub>max</sub> and specific surface area, H/C, O/C, and (O + N)/C are established (Fig. 5). The positive correlation between specific surface area and *Q*<sub>max</sub> confirmed the significant contribution of larger surface area

provided by BC colloids with higher pyrolysis temperature and smaller particle size to the higher adsorption capacity. The H/C, O/C, and (O + N)/C were all negatively correlated with *Q*<sub>max</sub>, indicating that high aromaticity and low polarity of BC colloids with high pyrolysis temperature favored the adsorption of organics.

### Desorption isotherms

Desorption isotherms of the three organics on BC colloids are shown in Fig. 4. The fitted adsorption parameters by the Freundlich and Langmuir models are given in Tables S5. The desorption isotherms of PHN and ATZ on BC colloids with all pyrolysis temperatures were almost overlapped with the corresponding adsorption isotherms (Fig. 4a, b), and the calculated HI values were all lower than 1, indicating the absence of desorption hysteresis for PHN or ATZ. It is known that no hysteresis can be defined when HI < 1 (Barriuso 1994). However, significant desorption hysteresis was observed for

**Table 1** Specific surface areas and pore volumes of BC colloids derived from bulk BCs with different pyrolysis temperatures and sizes

BC colloid	SA <sup>a</sup> (m <sup>2</sup> g <sup>-1</sup> )	A <sub>micro</sub> <sup>b</sup> (m <sup>2</sup> g <sup>-1</sup> )	PV <sup>c</sup> (cc g <sup>-1</sup> )	V <sub>micro</sub> <sup>d</sup> (cc g <sup>-1</sup> )	V <sub>meso</sub> <sup>e</sup> (cc g <sup>-1</sup> )
<b>250 nm</b>					
BC200	2.14	N.D	0.01	N.D	0.01
BC300	5.31	N.D	0.01	0.00	0.01
BC400	59.3	33.6	0.05	0.04	0.02
BC500	269	77.3	0.27	0.09	0.18
BC600	299	170	0.28	0.12	0.16
BC700	307	230	0.34	0.14	0.20
<b>500 nm</b>					
BC200	0.09	N.D	N.D	N.D	N.D
BC300	5.34	N.D	0.02	N.D	0.02
BC400	44.1	N.D	0.06	0.02	0.04
BC500	208	47.1	0.22	0.05	0.15
BC600	255	206	0.25	0.12	0.13
BC700	260	200	0.29	0.12	0.17
<b>1 μm</b>					
BC200	N.D	N.D	0.00	N.D	0.00
BC300	N.D	N.D	0.00	N.D	0.00
BC400	19.2	2.59	0.03	0.01	0.02
BC500	192	142	0.13	0.10	0.03
BC600	207	131	0.15	0.11	0.04
BC700	234	170	0.16	0.11	0.05

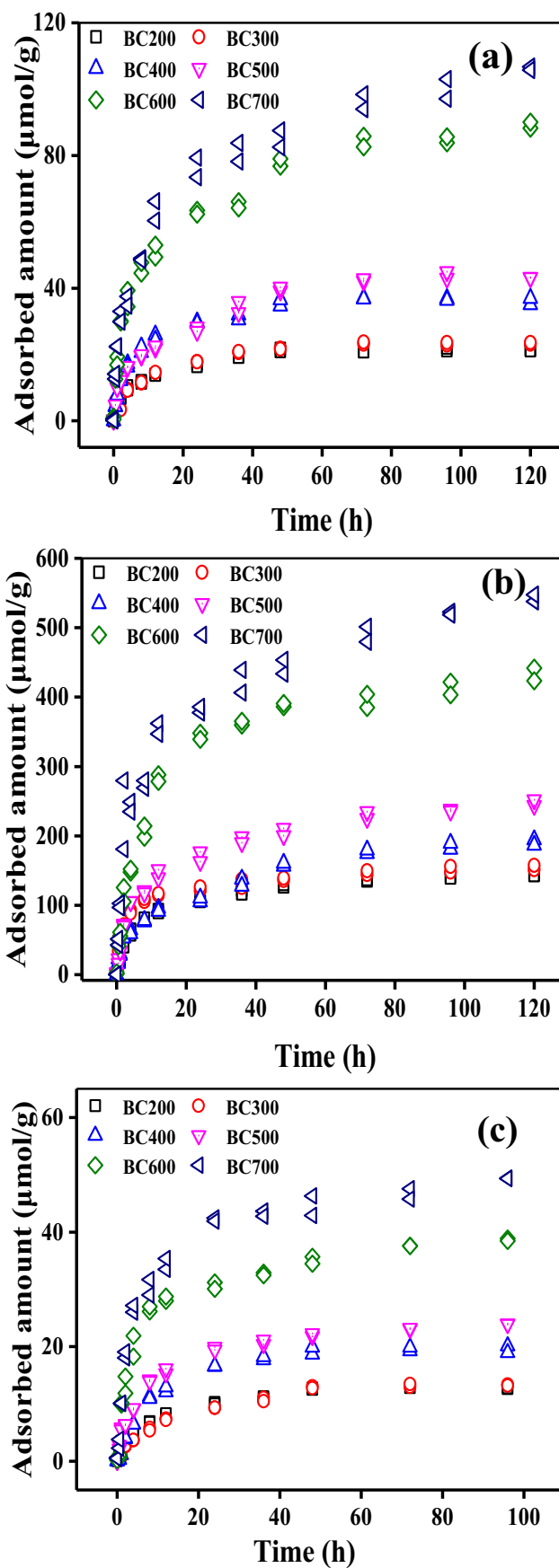
<sup>a</sup> SA surface area (m<sup>2</sup>/g)<sup>b</sup> A<sub>micro</sub> micropore surface area (m<sup>2</sup>/g)<sup>c</sup> PV pore volume<sup>d</sup> V<sub>micro</sub> micropore volume<sup>e</sup> V<sub>meso</sub> mesopore volume

OTC from BC colloids with the middle pyrolysis temperatures (300–500 °C) (Fig. 4c), and the highest HI was 3.20 for BC400 (1 μm) derived colloids.

### Adsorption-desorption mechanisms for the three organics

The adsorption of OTC, PHN, and ATZ on BC colloids from bulk BCs with different particle sizes and pyrolysis temperatures is schematically illustrated in Fig. 6. Possible main adsorption mechanisms rather than the general hydrophobic interaction are noted. Hydrophobic interaction can generally play a major role in the adsorption of organic chemicals on a surface in water (Apul and Karanfil 2015). OTC being the most hydrophilic as indicated by its lowest *K*<sub>ow</sub> (Table S1)

**Fig. 3** Adsorption kinetics of **a** PHN, **b** ATZ, and **c** OTC on BC colloids from BC<sub>1 μm</sub> with different pyrolysis temperatures. The adsorption kinetics of PHN, ATZ, and OTC on BC colloids from BC<sub>250 nm</sub> and BC<sub>500 nm</sub> are given in Figs. S4, S5, and S6 in SI, respectively



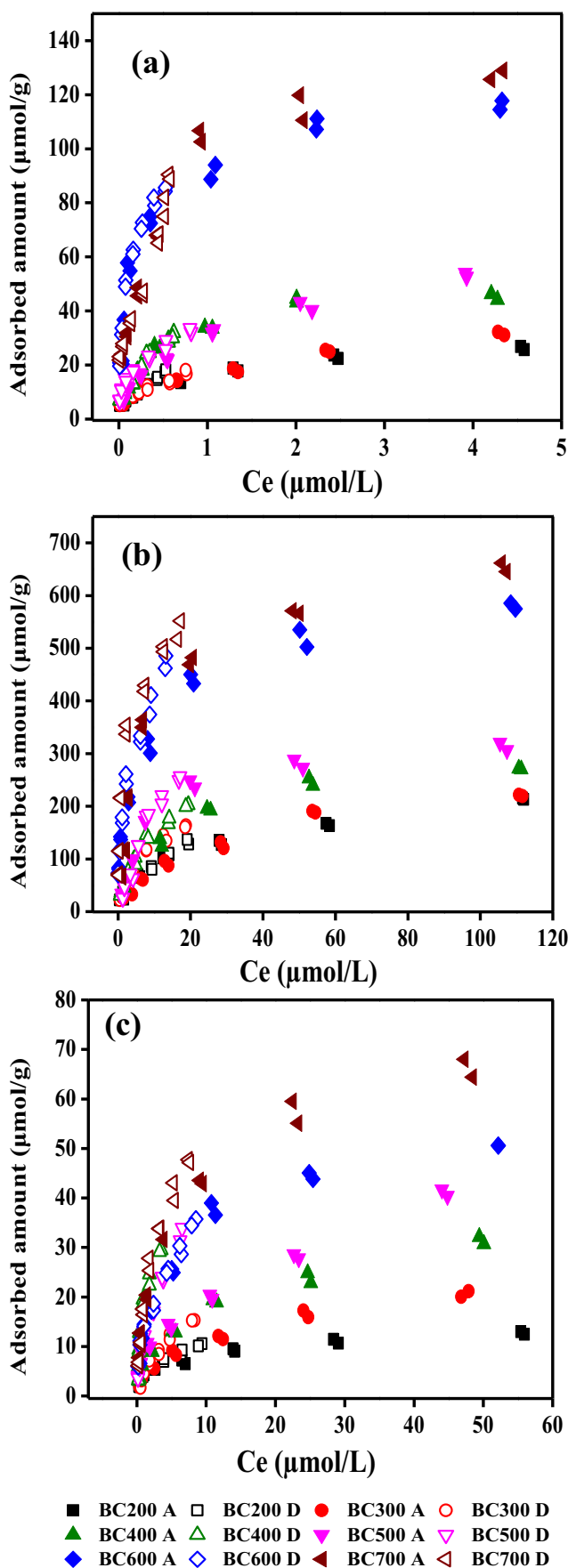


**Fig. 4** Adsorption and desorption isotherms of **a** PHN, **b** ATZ, and **c** OTC on BC colloids derived from BC<sub>1 µm</sub> with different pyrolysis temperatures. The letters A and D after BC<sub>200</sub>–BC<sub>700</sub> stand for adsorption and desorption, respectively. The adsorption isotherms of PHN, ATZ, and OTC on BC colloids from BC<sub>250 nm</sub> and BC<sub>500 nm</sub> are given in Figs. S7, S8, and S9 in SI, respectively

among the three organics could thus have the lowest  $Q_{max}$ . The  $\pi$ – $\pi$  stacking interaction between aromatic rings in PHN molecules and BC aromatic structures could contribute to the adsorption of PHN on BC particles (Lin et al. 2007; Chen et al. 2008; Yang et al. 2016). However, PHN possessing the highest  $K_{ow}$  exhibited much lower  $Q_{max}$  than ATZ, indicating other factors besides the hydrophobicity and aromaticity contributed to the adsorption. The high contents of minerals and oxygen-containing functional groups may form water cluster on BC colloid surfaces (Fu et al. 2018; Sun et al. 2013; Yang et al. 2018; Zhu et al. 2005), impeding the adsorption of hydrophobic organic contaminants like PHN. The higher adsorption capacity of ATZ than PHN could be ascribed to the stronger  $\pi$ – $\pi$  EDA interaction between ATZ and BC colloids. ATZ has a N-heterocyclic molecular structure, and the chlorine substituent in ATZ has electron-withdrawing nature, making the connected aromatic  $\pi$ -structures electron acceptors that interact with the aromatic carbon (electron-donors) on BC surfaces through  $\pi$ – $\pi$  EDA interactions (Keiluweit et al. 2010; Zhang et al. 2013; Lazar et al. 2013; Wang et al. 2015). The relatively largest molecule size of OTC could also partly explain its lowest adsorption by the porous structure of BC colloids. It was reported that the pore diameter should be 1.7 times greater than the widest dimension of adsorbate (Zhu et al. 2018; Li et al. 2017). Therefore, the pores with a diameter smaller than 15 Å would be inaccessible for tetracycline molecules (Li et al. 2019).

The observed desorption hysteresis for OTC indicated the occurrence of irreversible adsorption on BC colloids. Amidation reaction, an irreversible reaction, could occur between the amino group of OTC and the carboxyl/phenolic groups on BC colloid surfaces (Wu et al. 2013; Yang et al. 2019). Moreover, metals ions contained in BC colloids may form inner complexes with carboxylic and phenolic functional groups of OTC (Jia et al. 2013), contributing to the irreversible adsorption of OTC. BC colloids from BC<sub>300</sub>–500 were incompletely carbonized with instable pore development, making it possible that the porous structure swelled during adsorption and collapsed during desorption, which could also contribute to the desorption hysteresis (Wang et al. 2010).

### Conclusions

This study demonstrated that the specific surface area, pore volumes, aromatic clusters, and structural defects of BC colloids all increased with increasing pyrolysis temperature and



decreasing particle size. Pore diffusion was the main rate-determining step of the adsorption of organics by BC colloids. The adsorptions of PHN, ATZ, and OTC on BC colloids all increased with increasing pyrolysis temperature and decreasing particle size. The adsorption capacities of BC colloids for

the organics were positively related with the specific surface area, porosity, and aromaticity of BC colloids while negatively related with the polarity. The adsorptions of PHN and ATZ were all reversible, while desorption hysteresis occurred for OTC especially on BC colloids with the middle pyrolysis

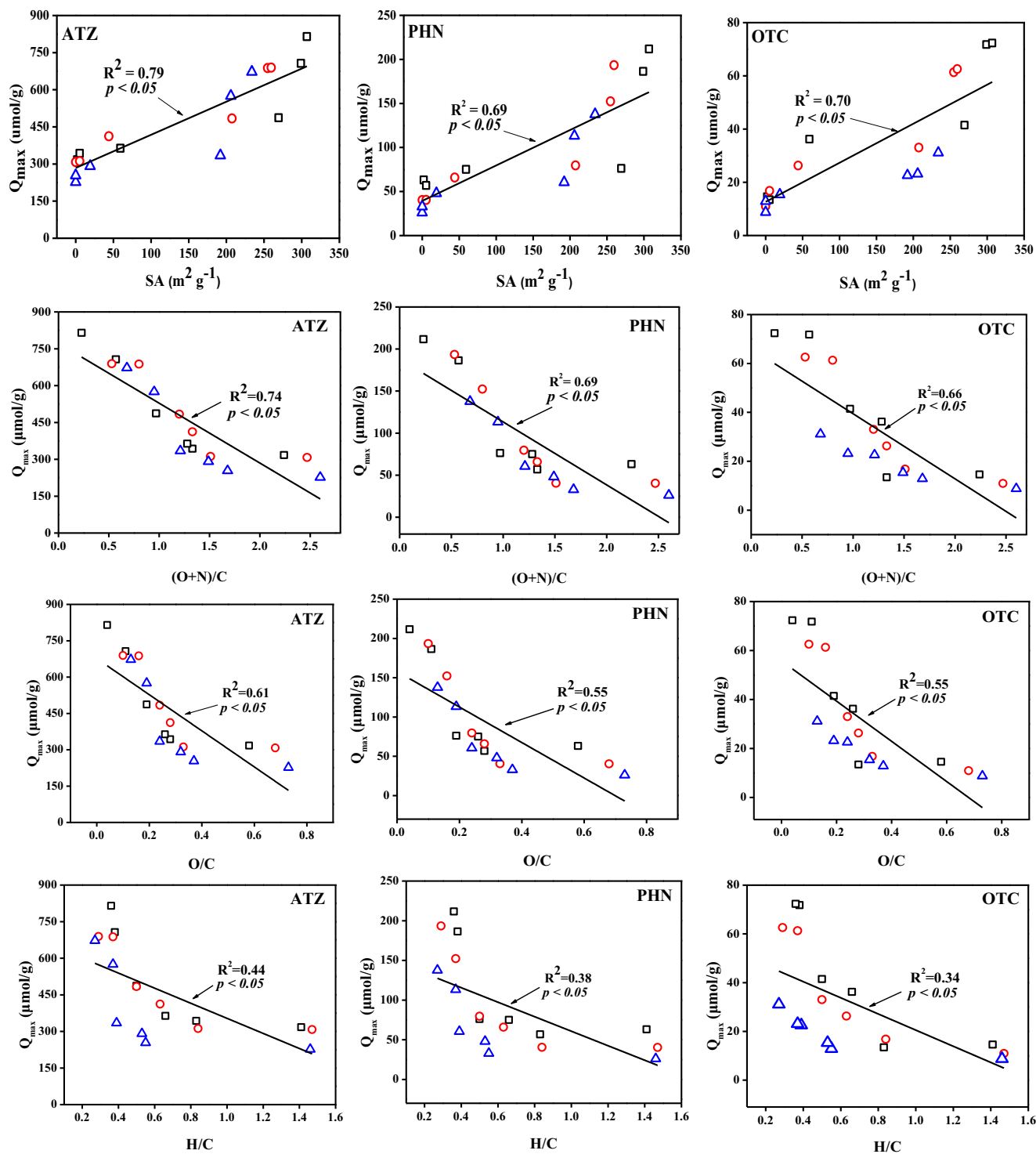


**Fig. 5** Linear correlations between specific surface area, (O + N)/C, O/C, and H/C of BC colloids with their adsorption capacities ( $Q_{\max}$ ) for ATZ, PHN, and OTC. Symbols  $\square$ ,  $\circ$ , and  $\Delta$  represent BC colloids from  $\text{BC}_{250 \text{ nm}}$ ,  $\text{BC}_{500 \text{ nm}}$ , and  $\text{BC}_{1 \mu\text{m}}$ , respectively.  $p < 0.05$  defined as significant

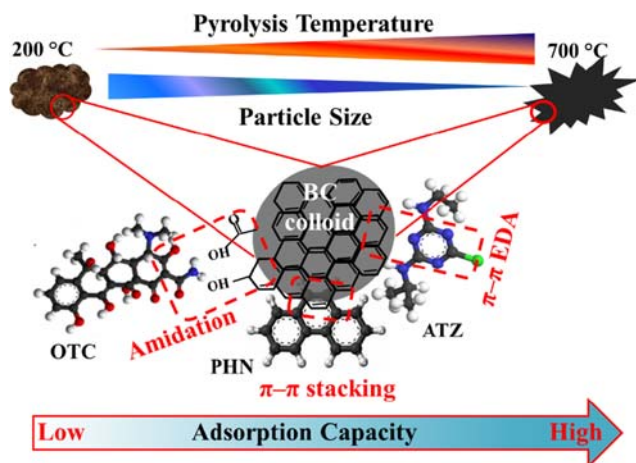


**Fig. 6** Schematic illustration of the adsorption of OTC, PHN, and ATZ on BC colloids from bulk BCs with different particle sizes and pyrolysis temperatures. Possible main adsorption mechanisms rather than the general hydrophobic interaction are noted

temperatures (300–500 °C). Hydrophobic interaction could play a major role in the adsorption, while the strong  $\pi$ – $\pi$  EDA interaction could occur between ATZ and BC colloids that resulted in the highest adsorption capacity for ATZ among the three organics. The inaccessibility of micropores in BC colloids may partly explain the lowest adsorption capacity for OTC with the largest molecular size and the highest hydrophilicity. Amidation reaction with carboxyl/phenolic groups on BC colloids, complexing with BC-contained metal ions, and/or pore collapse of incompletely carbonized BC colloids could cause the irreversible adsorption of OTC. These findings increase our knowledge on the adsorption behavior of BC colloids and will be helpful for assessing the environmental fate and risk of BC.

**Funding information** This work was supported by the National Key Research and Development Program of China (2017YFA0207003) and the National Natural Science Foundation of China (21621005 and 21525728).

## References

ASTM (1989) Standard methods for chemical analysis of wood charcoal. American Society for Testing and Materials, Philadelphia

Ahmad M, Rajapaksha AU, Lim JE, Zhang M, Bolan N, Mohan D, Vithanage M, Lee SS, Ok YS (2014) Biochar as a sorbent for contaminant management in soil and water: a review. *Chemosphere* 99: 19–33

Agrafioti E, Bouras G, Kalderis D, Diamadopoulos E (2013) Biochar production by sewage sludge pyrolysis. *J Anal Appl Pyrolysis* 101:72–78

Apul OG, Karanfil T (2015) Adsorption of synthetic organic contaminants by carbon nanotubes: a critical review. *Water Res* 68:34–55

Barriuso E (1994) Atrazine desorption from smectites. *Soil Sci Soc Am J* 58(6):1632–1638

Chen BL, Zhou DD, Zhu LZ (2008) Transitional adsorption and partition of nonpolar and polar aromatic contaminants by biochars of pine needles with different pyrolytic temperature. *Environ Sci Technol* 42:5137–5143

Ferrari AC (2007) Raman spectroscopy of graphene and graphite: disorder, electron–phonon fixed-bed column study. *Chem Eng J* 228: 496–505

Fu H, Wei C, Qu X, Li H, Zhu D (2018) Strong binding of apolar hydrophobic organic contaminants by dissolved black carbon released from biochar: a mechanism of pseudo micelle partition and environmental implications. *Environ Pollut* 232:402–410

Hameed R, Cheng LL, Yang K, Fang J, Lin DH (2019) Endogenous release of metals with dissolved organic carbon from biochar: effects of pyrolysis temperature, particle size, and solution chemistry. *Environ Pollut* 255(2):1–10

Huang W, Yu H, Weber WJ (1998) Hysteresis in the sorption and desorption of hydrophobic organic contaminants by soils and sediments. 1. A comparative analysis of experimental protocols. *J Contam Hydrol* 31:129–148

Ji L, Chen W, Duan L, Zhu D (2009) Mechanisms for strong adsorption of tetracycline to carbon nanotubes: a comparative study using activated carbon and graphite as adsorbents. *Environ Sci Technol* 43(7): 2322–2327

Jia M, Wang F, Bian Y, Jin X, Song Y, Kengara FO, Xu R, Jiang X (2013) Effects of pH and metal ions on oxytetracycline sorption to maize-straw-derived biochar. *Bioresour Technol* 136:87–93

Jones KD, Tiller CL (1999) Effect of solution chemistry on the extent of binding of phenanthrene by a soil humic acid: a comparison of dissolved and clay bound humic. *Environ Sci Technol* 33(4):580–587

Keiluweit M, Nico PS, Johnson MG, Kleber M (2010) Dynamic molecular structure of plant biomass-derived black carbon(biochar). *Environ Sci Technol* 44:1247–1253

Lazar P, Karlický F, Jurečka P, Kocman M, Otyepková E, Šafářová K, Otyepka M (2013) Adsorption of small organic molecules on graphene. *J Am Chem Soc* 135:6372–6377

Lehmann J, Joseph S (2009) Biochar for environmental management: science and technology. Earthscan Publications Ltd., London

Li Y, Li M, Li Z, Yang L, Liu X (2019) Effects of particle size and solution chemistry on triclosan sorption on polystyrene microplastic. *Chemosphere* 231:308–314

Li S, Lü J, Zhang T, Cao Y, Li Y (2017) Relationship between biochars' porosity and adsorption of three neutral herbicides from water. *Water Sci Technol* 75:482–489

Lin DH, Pan B, Zhu LZ, Xing BS (2007) Characterization and phenanthrene sorption of tea leaf powders. *J Agric Food Chem* 55:5718–5724

Liu G, Zheng H, Jiang Z, Zhao J, Wang Z, Pan B, Xing B (2018) Formation and physicochemical characteristics of nano biochar: insight into chemical and colloidal stability. *Environ Sci Technol* 52(18):10369–10379

Liu Z, Zhang FS, Wu J (2010) Characterization and application of chars produced from pyrolysis and hydrothermal treatment. *Fuel* 89:510–551

Major J, Lehmann J, Rondon M, Goodale C (2010) Fate of soil-applied black carbon: downward migration, leaching and soil respiration. *Glob Chang Biol* 16:1366–1379

Mukherjee S, Weiermüller L, Tappe W, Hofmann D, Köppchen S, Laabs V, Vereecken H, Burauel P (2016) Sorption–desorption behaviour of bentazone, boscalid and pyrimethanil in biochar and digestate based soil mixtures for biopurification systems. *Sci Total Environ* 559:63–73

- Oleszczuk P, Pan B, Xing BS (2009) Adsorption and desorption of oxytetracycline and carbamazepine by multiwalled carbon nanotubes. *Environ Sci Technol* 43:9167–9173
- Qian L, Zhang W, Yan J, Han L, Gao W, Liu R, Chen M (2016) Effective removal of heavy metal by biochar colloids under different pyrolysis temperatures. *Bioresour Technol* 206:217–224
- Qu XL, Fu HY, Mao JD, Ran Y, Zhang DN, Zhu DQ (2016) Chemical and structural properties of dissolved black carbon released from biochars. *Carbon* 96:759–767
- Schlautman MA, Morgan JJ (1993) Effects of aqueous chemistry on the binding of polycyclic aromatic hydrocarbons by dissolved humic materials. *Environ Sci Technol* 27(5):961–969
- Spokas KA, Novak JM, Masiello CA, Johnson MG, Colosky EC, Trigo JA, Trigo C (2014) Physical disintegration of biochar: an overlooked process. *Environ Sci Technol Lett* 1:326–332
- Sun W, Yin K, Yu X (2013) Effect of natural aquatic colloids on Cu (II) and Pb (II) adsorption by Al<sub>2</sub>O<sub>3</sub> nanoparticles. *Chem Eng J* 225:464–473
- Wang XL, Xing B (2007) Sorption of organic contaminants by biopolymer-derived chars. *Environ Sci Technol* 41:8342–8348
- Wang Y, Li Y, Kim H, Walker SL, Abriola LM, Pennell KD (2010) Transport and retention of fullerene nanoparticles in natural soils. *J Environ Qual* 39(6):1925–1933
- Wang D, Zhang W, Hao X, Zhou D (2013) Transport of biochar particles in saturated granular media: effects of pyrolysis temperature and particle size. *Environ Sci Technol* 47:821–828
- Wang S, Gao B, Zimmerman AR, Li Y, Ma L, Harris WG, Migliaccio KW (2015) Physicochemical and sorptive properties of biochars derived from woody and herbaceous biomass. *Chemosphere* 134:257–262
- Wang P, Tang L, Wei X, Zeng G, Zhou Y, Deng Y, Wang J, Xie Z, Fang W (2017) Synthesis and application of iron and zinc-doped biochar for removal of p-nitrophenol in wastewater and assessment of the influence of co-existed Pb(II). *Appl Surf Sci* 392:391–401
- Wu L, Lin L, Gao B, Rafael MC, Zhang M, Chen H, Zhou Z, Wang H (2013) Aggregation kinetics of graphene oxides in aqueous solutions: experiments, mechanisms, and modelling. *Langmuir* 29:15174–15181
- Xie M, Chen W, Xu Z, Zheng S, Zhu D (2014) Adsorption of sulfonamides to demineralized pine wood biochars prepared under different thermochemical conditions. *Environ Pollut* 186:187–194
- Yah LG, Qin LL, Yu HQ, Li S, Shan RR, Du B (2016) Adsorption of acid dyes from aqueous solution by CTMAB modified bentonite: kinetic and isotherm modeling. *J Mol Liq* 211:1074–1081
- Yang K, Yang JJ, Jiang Y, Wu WH, Lin DH (2016) Correlations and adsorption mechanisms of aromatic compounds on a high heat temperature treated bamboo biochar. *Environ Pollut* 210:57–64
- Yang K, Jiang Y, Yang J, Lin DH (2018) Correlations and adsorption mechanisms of aromatic compounds on biochars produced from various biomass at 700 °C. *Environ Pollut* 233:64–70
- Yang L, Zhao H, Liu N, Wang W (2019) A target analyte induced fluorescence band shift of piperazine modified carbon quantum dots: a specific visual detection method for oxytetracycline. *Chem Commun* 82(55):12364–12367
- Zhang P, Sun H, Yu L, Sun T (2013) Adsorption and catalytic hydrolysis of carbaryl and atrazine on pig manure-derived biochars: impact of structural properties of biochars. *J Hazard Mater* 244–245:217–224
- Zhang P, Sun H, Yu L, Sun T (2012) Adsorption and catalytic hydrolysis of carbaryl and atrazine on pig manure-derived biochars: impact of structural properties of biochars. *J Hazard Mater* 245:217–224
- Zhang W, Niu J, Morales VL, Chen X, Hay AG, Lehmann J, Steenhuis TS (2010) Transport and retention of biochar particles in porous media: effect of pH, ionic strength, and particle size. *Ecohydrology* 3(4):497–508
- Zhao X, Ouyang W, Hao F, Lin C, Wang F, Han S, Geng X (2013a) Properties comparison of biochars from corn straw with different pretreatment and sorption behaviour of atrazine. *Bioresour Technol* 147:338–344
- Zhao X, Ouyang W, Hao F, Lin C, Wang F, Han S, Geng X (2013b) Properties comparison of biochars from corn straw with different pretreatment and sorption behaviour of atrazine. *Bioresour Technol* 147:338–344
- Zhu DQ, Kwon S, Pignatelli JJ (2005) Adsorption of single-ring organic compounds to wood charcoals prepared under different thermochemical conditions. *Environ Sci Technol* 39:3990–3999
- Zhu D, Pignatello JJ (2005) Characterization of aromatic compound sorptive interactions with black carbon (charcoal) assisted by graphite as a model. *Environ Sci Technol* 39:2033–2041
- Zhu X, Li C, Li J, Xie B, Lü J, Li Y (2018) Thermal treatment of biochar in the air/nitrogen atmosphere for developed mesoporosity and enhanced adsorption to tetracycline. *Bioresour Technol* 263:475–482

**Publisher's note** Springer Nature remains neutral with regard to jurisdictional claims in published maps and institutional affiliations.